Proceedings of the Sixth International Conference on
Railway Technology: Research, Development and Maintenance
Edited by: J. Pombo
Civil-Comp Conferences, Volume 7, Paper 2.4
Civil-Comp Press, Edinburgh, United Kingdom, 2024
ISSN: 2753-3239, doi: 10.4203/ccc.7.2.4

Effect of Hardness and Temperature on Wheel-Rail Wear: Theoretical and Experimental Study

Z. Shi, E. Meli, L. Nencioni and A. Rindi

**Department of Industrial Engineering of Florence (DIEF),
University of Florence
Italy**

Abstract

This paper extends the modelling approach towards the evaluation of wear, by including the effect of rail/wheel hardness ratio and ambient temperature. We firstly perform wear tests in the laboratory with varied hardness ratios from 0.79 to 1.60, and different ambient temperature from -40 to 20 degree. Then we formulated the new wear laws and determined corresponding coefficients in the formulas. The proposed new wear laws are validated through a numerical example based on a prediction model. Comparison between the simulated results and in-field results shows that the results from the simulation are well consistent with those from field measurements.

Keywords: wear, hardness, temperature, railway, modelling, tests.

1 Introduction

The railway system is subject to complex conditions, with the wheel and rail surfaces in relative motion and exposed to an open environment [1]. These surfaces undergo physical and chemical changes that degrade their performance, such as reduced wear resistance, fatigue cracks, corrosion, etc. Over the past few years, researchers have carried out numerous investigations to explore the relationship between wear and surrounding variables. The roles of several variables in different categories can be found, such as environmental conditions (humidity, precipitation, temperature, etc.) [1], dynamical indicators (sliding velocity, creepage, contact pressure, etc.) [2–4], and material characteristics (hardness, roughness, etc.) [5].

The effect of hardness ratio on wear mechanism through experiments was investigated in [6]. It was found that hardness ratio caused a transition of the wear and RCF damage mechanisms on the wheel–rail steels. However, the constants in classical wear laws are usually delivered from limited combinations of materials. The modelling of wear that takes the influence of hardness ratio into consideration has not been addressed sufficiently. Therefore, it is necessary to look for the new wear and RCF laws that consider the variation of hardness ratio. On the other hand, various environmental conditions significantly impact the wheel/rail contact interface, leading to these types of damage. Factors such as humidity, precipitation, and ambient temperature play substantial roles in causing interface damage [2–4]. Ambient temperature is particularly crucial as it directly affects many physical and chemical attributes of wheel and rail materials, like hardness, strength, toughness, and oxidation rate, thereby changing the frictional behaviour and the wear mode and rate between the wheel and rail [5]. In recent years, a number of experiments have been conducted to investigate the impact of low-temperature environments on wheel–rail damage, yielding valuable insights [7,8]. Research has shown that at temperatures of −30 ◦C and 50 ◦C, the wear loss of both the wheel and rail is higher compared to that at room temperature [9]. However, at −40 ◦C, the wear rate of the wheel and rail is lower than that at room temperature, with the difference being more noticeable in the case of the rail [10]. The carbon content of the material has differing effects on the wear rate of the wheel and rail at room temperature and −40 ◦*C* [11]. The change in temperature can cause various effects and lead to different phenomena. In terms of wear, it is widely accepted that temperature and humidity have an interactive effect in a specific environment. Temperature plays a crucial role in the oxidation process, which in turn affects the occurrence of different types of wear, such as oxidation wear or abrasive wear. The carbon content of a single material, hardness value, and hardness ratio of a pair of materials can all affect the speed at which this process occurs. Qualitative investigations through tests and scanning electron microscope (SEM) observations have preliminarily revealed the mechanisms of this process in published works [10,12]. These may form the basis for advancing research on wear mapping investigations, particularly through innovative extensions of classic laws, to enable more accurate predictions of wear in railway lines.

In this paper, we aim to present our recent investigation on new wear models considering the effect of rail/wheel hardness ratio and ambient temperature [22-24]. We conducted laboratory tests under different operating conditions to collect data, and based on this data, we propose new laws to describe the relationship between wear rate and wear index, considering the effect of ambient temperature and hardness ratio. Section 2 introduces the experimental laboratory results on which the new wear laws are based. In Section 3, we provide detailed results, discussions, and proposed new expressions that consider the effects of the hardness ratio and temperature. We applied these new wear laws in a wear prediction model using a railway line as an example, as discussed in Section 4. Our work contributes to the development of more accurate and comprehensive wear evaluation laws for railway wheels and rails, considering the effect of rail/wheel hardness ratio and ambient temperature.

2 Methods

The experiments were carried out through multiple apparatuses, which can be used to study the effects of different parameters on rolling friction and wear tests of wheel-rail materials under various contact conditions. Figure 1 illustrates a schematic diagram of MJP-30A twin-disc apparatus. The apparatus allows the discs to run against each other with controlled normal and tangential forces to reproduce the rolling-sliding contact of wheel and rail. The hardness values of corresponding wheel and rail materials are shown in Table 1. The summary of experimental temperature parameter is listed in Table 2. For the hardness test, to investigate each pair of the wheel-rail materials in Table 1, 3-10 couples of wheel-rail samples were obtained. Each couple of wheel and rail rollers were cut from the wheel tread surface and the rail top surface through wire cutting. All rollers were turned and ground into the diameter of 50 mm. The width of rail rollers is 10 mm while 5 mm for wheel rollers, leading to a contact width of 5 mm. Then, these samples were mounted in the resin and ground with sandpaper, polished with paste and etched with 4% Nital. Before and after the rolling-sliding tests, the rail rollers were ultra-sonically cleaned in ethyl alcohol. Then the mass of the rollers was measured using an electronic balance (JA4103, accuracy: 0.0001g). In the discs tests for temperature, to realize various temperature conditions, a cooling system and an environmental chamber were equipped. The cooling system is able to provide the lowest temperature of -60°C. Before the rolling-sliding test, the temperature in the environmental chamber was pre-cooled to the desired value and maintained for 2 hours to make sure that both the wheel and the rail rollers achieved a uniform temperature. A PID temperature controller was used to stabilize the temperature inside the environment chamber at the set value and the variation of temperature was less than 2°C. A temperature-humidity sensor was installed in the environment chamber so that the temperature and relative humidity could be monitored. The normal load was applied through a spring. A torque sensor (TQ660, 0~ 20 $N•m$) was installed on the lower shaft to record the tangential force.

Wheel grade	Wheel hardness	Rail grade	Rail hardness	Hardness ratio (Hr/Hw)
C-class	388	U75V	319	0.82
C-class	354	PG5	405	1.14
C-class	354	U22SiMn	451	1.27
D-class	345	U75V	290	0.84
CL60	327	U75V	319	0.98
CL60	320	U75V	290	0.91
ER7	296	U75V	319	1.08
CL60	280.56	U71Mn	300.78	1.07
CL60	280.56	U75V	320.69	1.14
CL60	280.56	U71MnH	328.48	1.17
CL60	280.56	U75VH	358.93	1.28

Table 1: Summary of wear test conditions: hardness.

Wheel grade	Hardness	Rail grade	Hardness	Hardness ratio (Wheel/Rail)	T(°C)
ER9	289	U71Mn	278	0.96	-40,20
ER8	254	U71Mn	278	1.09	-40,-30,-15,20
ER9	255	U75v	303	1.19	-40,20
ER8	254	PG5	406	1.60	-40,20
ER8	254	PG4	389	1.53	-40,20

Table 2: Summary of wear test conditions: temperature.

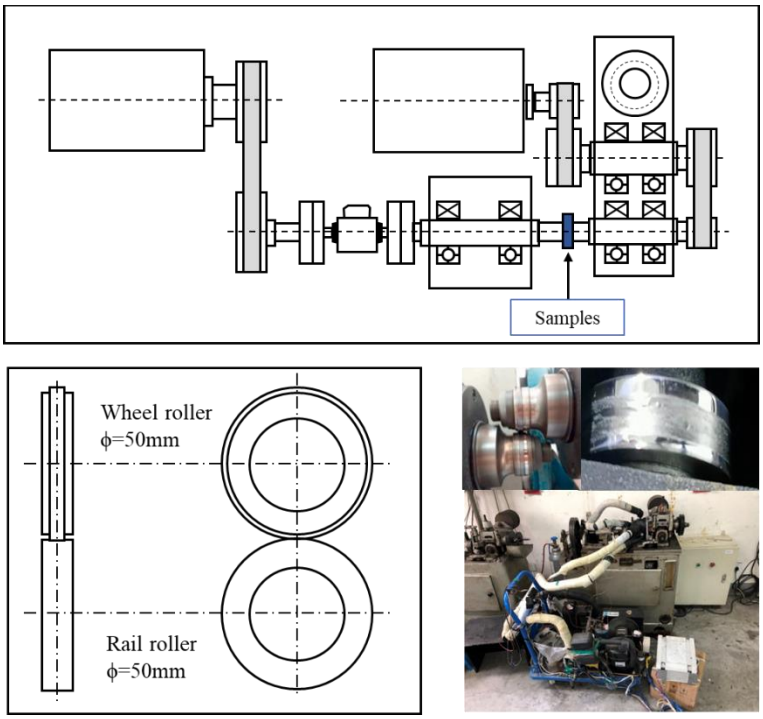

Figure 1: Schematic diagram of the twin-disc test apparatus: MJP-30A

3 Results

3.1 Hardness

Figure 2 shows the resulted wear rate changing with wear index Tγ/A(the product of traction force T and slip ratio γ divided by contact area A), from a twin-disc test using CL60 wheel and U75V rail material. For current test, the slip ratio used is in the range from 0.5% to 25%. 7 pairs of wheel-rail disc samples were used. The velocity of the wheel disc is faster than the rail disc. The wheel disc drives the rail disc. The contact pressure between wheel and rail rollers is 1500 MPa.

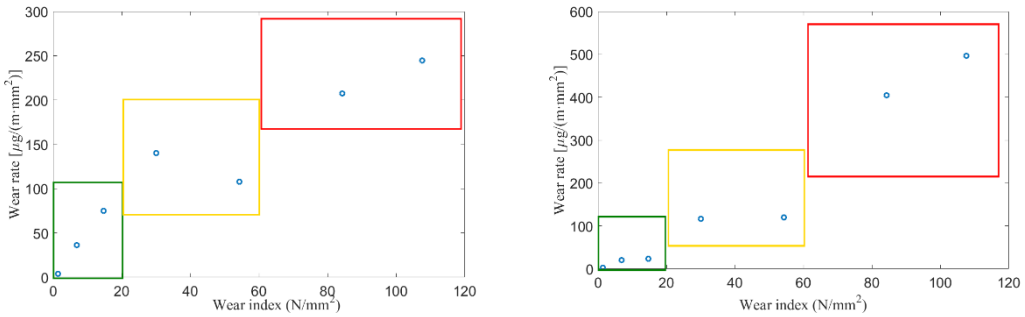

Figure 2: Wear mapping from twin-disc tests using CL60 wheel and U75V rail material (a) CL60 wheel; (b)U75V rail.

In the Figure 2, three wear regimes (K1-mild wear, K2-severe wear, and K3-catastrophic wear) are mapped for the wheel and the rail, respectively. It is seen that, for the current wheel and rail, in mild and severe regimes, rail material (U75V-290) is worn less than wheel material (CL60-320); but in the catastrophic regime, rail material (U75V-290) is worn more than wheel material (CL60-320). This implies that the wear mechanism in catastrophic regime is different from that in mild and severe regimes. Further analysis on the mechanism reveals that the dominating wear type transformed from oxidative wear to fatigue wear. The wear mapping with a group of various hardness ratio materials is shown in Figure 3. As the hardness ratio increases from 0.82 to 1.17, the material with higher wear rate switched from the rail to the wheel. The results plotted in Figure 4 summarize the wear mapping in mild regimes for the wheel and the rail. It is obvious that the laws for wheel and rail are inconsistent, which indicates that the quantitative investigation must be discussed separately for the wheel and the rail.

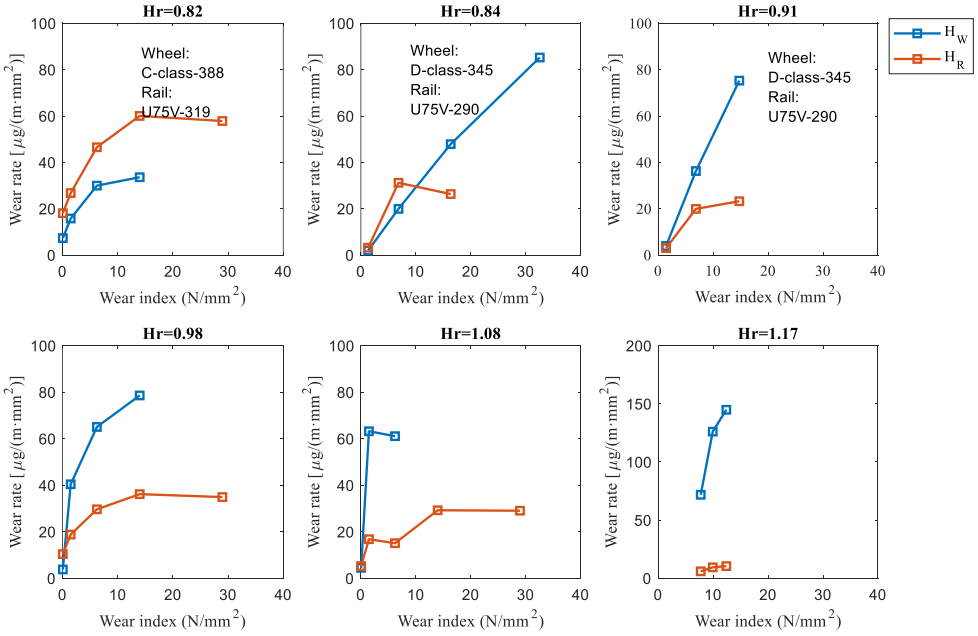

Figure 3: Wear mapping from twin-disc tests using materials with various hardness ratio

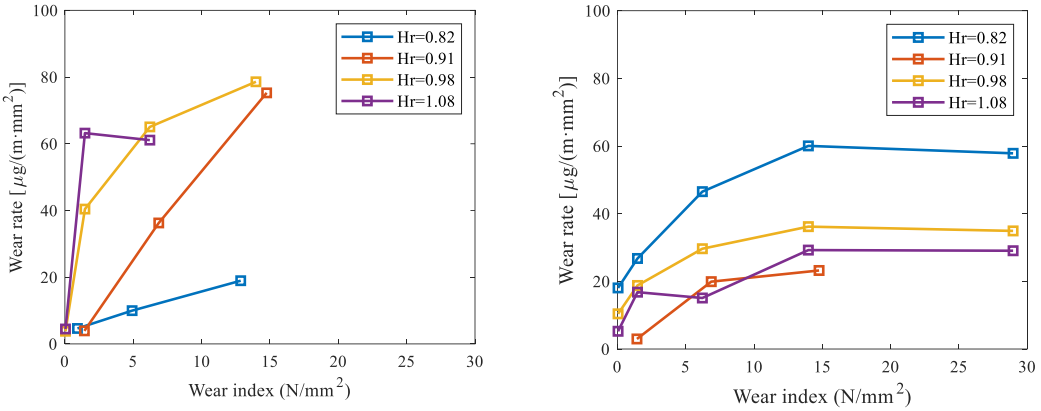

Figure 4: Wear mapping from twin-disc tests using materials with various hardness ratio (a) wheel; (b) rail.

Through the experimental results (as shown in Figure 1), it is possible to determine the value of K1 in mild wear regime for current case. In this paper, the value of K1 is determined by curve-fitting data in the mild regime and solved with the method of least squares. We define $K_1^{\,w}$ and $K_1^{\,r}$ as the coefficients for wheel and rail in the mild regime of the wear map. We could determine the values of $K_{1i}^{\,w}$ and $K_{1i}^{\,r}$ for different hardness ratios. In Figure 5, the results $K_{1i}^{\,w}$, $K_{1i}^{\,r}$ and the fitting curves are shown. We assume the above wheel and rail material pairing in Figure 2 as the reference case. We propose the new wear law by introducing the effect of hardness ratio, as expressed in the following equations:

$$\begin{cases} K_1^{\,w} = f_w(Hr)\cdot K_{1_0}^{\,w}\cdot\dfrac{T\gamma}{A} & \dfrac{T\gamma}{A} < I_0 \\ K_2^{\,w} = f_w(Hr)\cdot K_{1_0}^{\,w}\cdot I_0^{w} & \dfrac{T\gamma}{A} \geq I_0 \end{cases} \tag{1}$$

$$\begin{cases} K_1^{\,r} = f_r(Hr)\cdot K_{1_0}^{\,r}\cdot\dfrac{T\gamma}{A} & \dfrac{T\gamma}{A} < I_0 \\ K_2^{\,r} = f_r(Hr)\cdot K_{1_0}^{\,r}\cdot I_0^{r} & \dfrac{T\gamma}{A} \geq I_0 \end{cases} \tag{2}$$

$$\begin{cases} f_w(Hr) = a_w\left(1-b_w e^{-c_w Hr}\right) \\ f_r(Hr) = a_r e^{b_r Hr} \end{cases} \tag{3}$$

where a_w , b_w , c_w , a_r and b_r are functional parameters to be tuned. The results are shown in Table 3.

Wheel case	Value	Rail case	Value
a_w	4.6185	a_r	14.3282
b_w	3.5597	b_r	-2.8910
c_w	1.6554	/	

Table 3: Values of wear constant for wheel and rail.

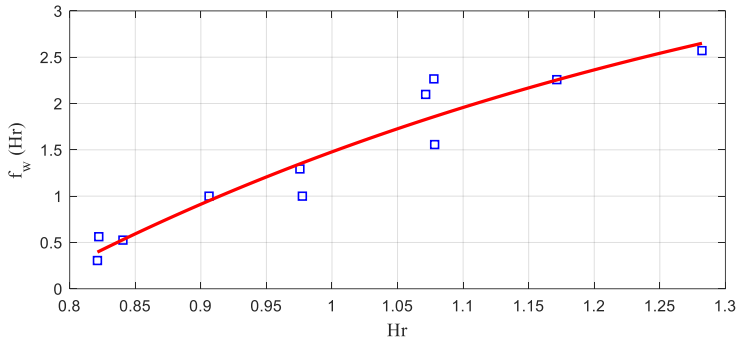

(a)

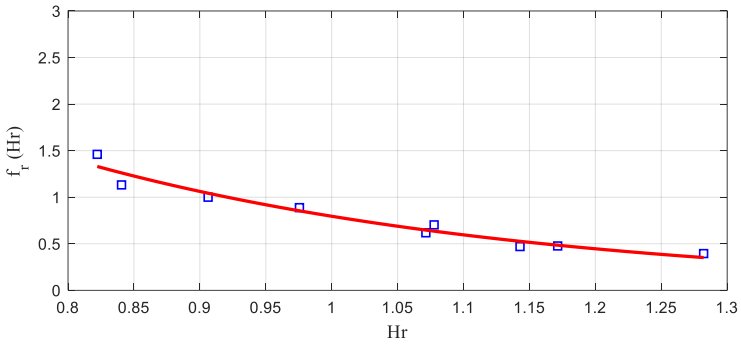

(b)

Figure 5: Experimental results- wear constants: (a) wheel; (b) rail.

3.2 Temperature

Figure 6 shows an example, which plots the resulted wear rate changing with wear index Tγ/A, from a twin-disc test using ER9 wheel and U75V rail material. For the current test, the slip ratio used is in the range of 0.17% to 9.43%. The velocity of the wheel disc is faster than the rail disc. The contact pressure between wheel and rail rollers is 566.5 MPa. It is seen that the wear rate of ER9-wheel and U71Mn-Rail under different temperatures varies significantly.

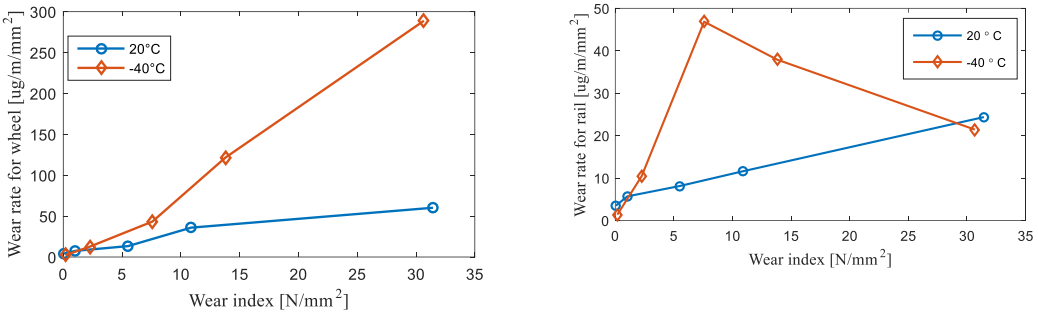

(a) (b)

Figure 6: Wear characteristic of ER9 wheel steel coupled with U71Mn rail steel at + 20 ° C and -40 ° C: (a) wheel wear. (b) rail wear

Modelling of the catastrophic and severe regimes may be distorted due to the lack of sufficient experimental data, in the current paper, we focus on the wear only in the mild regime, excluding the catastrophic and the severe regimes. As plotted in Figure 2(a) for the wheel wear, the wear coefficient at low temperature is higher than that at room temperature. The same trend can be seen for the rail, in Figure 6(b). Another consideration that we can make regarding this case shown in Figure 6(a) is that, while at room temperature, upon reaching a certain wear index value, a stabilization of the wear rate is observed, linked to the transition from the region of light wear to severe wear, when at -40 ° C this behaviour variation is not observed and the wear rate continues to increase in the whole field of dissipated power. In Figure 6(b), although there is a greater dispersion of the experimental data, the considerations seen on the wheel side are confirmed. By lowering the temperature there is an increase in wear rate with the same Wear Index, at least with regards to the field of mild wear. This behaviour can be motivated by the fact that the lowering of temperature induces net embrittlement of the material and therefore leads to the detachment of micro-roughness from the wheel and rail surfaces. These while at room temperature, when the material is more ductile, they tend to deform plastically, under the action of the loads exchanged at the interface, with the lowering of the temperature and the embrittlement of the material instead tend to break and consequently favour the detachment of some portions of material from the surfaces. According to the wear function proposed in [9,10], the slope of fitted data in the mapping plot can be calculated. The resulted value of the slopes is listed in Table 4.

Wear coefficient in the mild regime	**Values**	**Temperature**
K_1^w	8.0501	-40° C
K_1^r	6.0552	
K_1^w	3.1536	20° C
K_1^r	1.6170	

Table 4 Resulted value of K_1 at different conditions (ER9-wheel vs U71Mn-rail)

In the table, K_1^w and K_1^r represent the slope in wear mapping plots for the wheel and the rail, while the physical quantity of the coordinate axis in the wear rate v.s. wear

index $T\gamma / A$ with the units of [$\mu g / m / mm^2$] and [N / mm^2] respectively. In this paper, the slope of wear rate- wear index $T\gamma / A$ lines in the mild wear regime, K1 as shown in Figure 6, is used to describe the significant characteristic of the material during the wear process. Correspondingly, values of K1 under different test conditions can be calculated. Figure 7 plots the K1 (slope in mild wear regime) at different hardness ratios and temperatures.

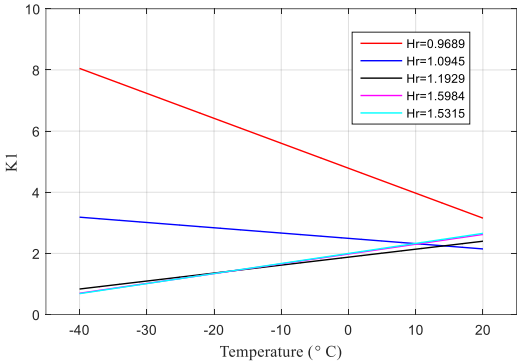

(a)

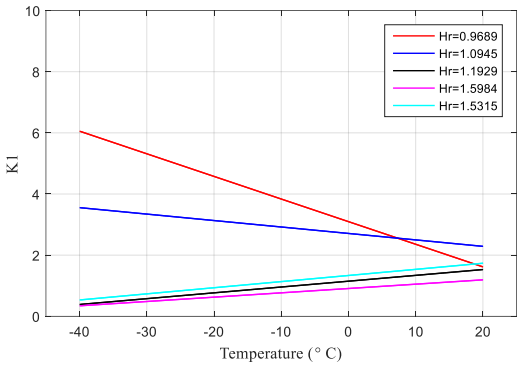

(b)

Figure 7. K1- (slope in the mild wear regime) at different hardness ratios and temperatures: (a) wheel (b) rail

Figure 7 shows how the slope of the linear section of the wear characteristic varies with temperature. Due to the limited amount of data, Figure 7 summarizes the results with the range of 0.97 to 1.53 for the hardness ratio, and -40 and 20 °C for the temperature. It is seen that at a low hardness ratio, K1 is more sensitive to the temperature. The slope of the lines in Figures 7(a) and 7(b) are found significant correlation with the hardness ratio. For pairs of materials that have a lower hardness ratio and less than 1, the reduction in temperature leads to an increase in the slope of the wear characteristic. If, on the other hand, the hardness ratio of the materials involved increases to about 1, then the slope of the lines seems to cancel out and this means that the materials wear out equally at both low and high temperatures. Finally, when the Hardness ratio reaches values close to about 1.2, the slope of the curves stops growing and saturates at a rather constant value. One of the reasons why this phenomenon could be explained is the embrittlement of the material as a direct consequence of the lowering of temperature. If the material at room temperature is

ductile because it has a hardness that is not too important, by lowering the temperature it will tend to become more brittle and therefore we will observe an increase in the wear rate linked to the detachment of the micro-asperities from the surface. However, if the material is particularly hard even at room temperature, the lowering of temperature leads to an increase in hardness such that the wear mechanisms tend to almost cancel out.
To describe this trend between the slope of K1-temperature line, m(Hr), and the hardness ratio, Figure 8 plots the relationship for the wheel and the rail.

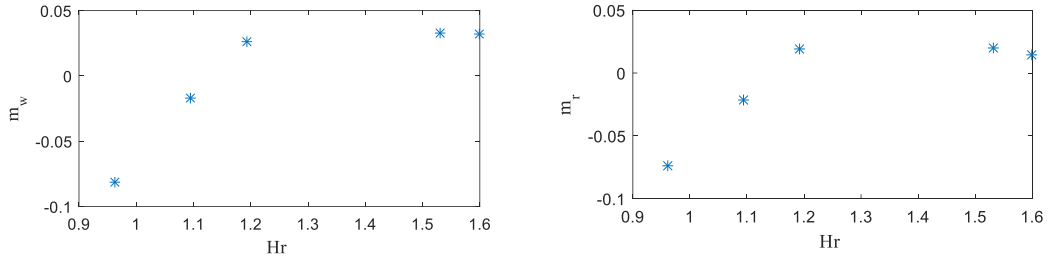

(a) (b)

Figure 8: Trend of the coefficient m as a function of Hr (a) wheel (b) rail

To introduce this phenomenon into the wear characteristic, we proposed the following equations:

$$K_{1_{wheel}} = f_w(Hr) \cdot f_w(T) \cdot K_{1_0}^w \cdot \frac{T\gamma}{A} \tag{2}$$

$$K_{1_{rail}} = f_r(Hr) \cdot f_r(T) \cdot K_{1_0}^r \cdot \frac{T\gamma}{A} \tag{3}$$

where

$$f_w(Hr) = a_w \cdot (1 - b_w e^{-c_w \cdot Hr}) \tag{4}$$

$$f_w(T) = \frac{f_w(Hr) \cdot K_{1_0}^w + m_w(Hr) \cdot (T - 20)}{f_w(Hr) \cdot K_{1_0}^w} \tag{5}$$

$$f_r(Hr) = a_r \cdot e^{-b_r \cdot Hr} \tag{6}$$

$$f_r(T) = \frac{f_r(Hr) \cdot K_{1_0}^w + m_r(Hr) \cdot (T - 20)}{f_r(Hr) \cdot K_{1_0}^r} \tag{7}$$

While according to the results, we have the following fitting results:

$$a_w = 4.6185$$
$$b_w = 3.5597$$
$$c_w = 1.6554$$
$$K_{1_0}^w = 5.1135$$

$$a_r = 14.3282$$

$$b_r = -2.897$$

$$K_{1_0}^r = 1.8111$$

$$\begin{cases} m_w(Hr) = m_{1_w} \cdot Hr + m_{2_w} & Hr < 1.2 \\ m_w(Hr) = m_{3_w} & Hr > 1.2 \end{cases}$$

with

$$m_{1_w} = 0.4671$$

$$m_{2_w} = -0.5302$$

$$m_{3_w} = 0.0303$$

$$\begin{cases} m_r(Hr) = m_{1_r} \cdot Hr + m_{2_r} & Hr < 1.2 \\ m_r(Hr) = m_{3_r} & Hr > 1.2 \end{cases}$$

with

$$m_{1_r} = 0.4015$$

$$m_{2_r} = -0.4613$$

$$m_{3_r} = 0.0217$$

Note that Equations 2-7 are proposed based on the current limited data sample. This limitation may restrict the accuracy of the formula and model, and more data volume may improve the model. With more data, the determination of the coefficients will be changed accordingly.

4 Validation

In the current study, we focus on the validation of wheel wear evolution, using collected reliable data about the wear of wheel and rail, from a metro line. Numerical simulation is performed based on developed prediction models. The general architecture of the prediction model is shown in Figure 9. As it depicts, two main parts are included, the dynamics model and the wear model. Kinematic variables, contact points and forces are transferred between the vehicle track coupled model and the global contact model. Based on the results from the dynamics model, the local contact variables can be calculated, and then local contact variables are further passed to wear evaluation models. The wear evaluation procedures are based on the aforementioned models. The wear evaluation model estimates the removed material from the profiles of the wheel and rail.

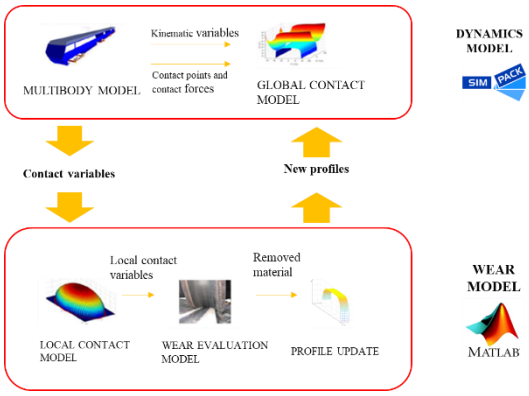

Figure 9: A general architecture of the established wear prediction model.

Here we briefly introduce how to implement the wear update strategy. In the simulation model, we assume that, inside each discrete unit, the wear quantity is close to linear with the travelled distance. This requires the unit length small enough to neglect the profile variation between two consequent units. In this way, the total length is discretized by a series of unit lengths, and each unit length is discretized by a series of track lengths. Mark the total mileage of the worn vehicle as total length km_{tot}, the unit length inside each discrete unit as km_{unit} , and the track length for each simulation inside one unit as l_{track}. Figure 10 illustrates the discretization of the total mileage.

Figure 10: Discretization of the total mileage

It is possible to amplify the removed material during the dynamic simulations by means of a scaling factor which increases the distance traveled by the vehicle. Similarly, for the rail, we assume that the wear is proportional to the total tonnage burden on the track. Marked the total tonnage of the rail as M_{tot} , and to the total number of vehicles operating on the line, marked as N_{tot} . In this way, the total tonnage is represented by the total number, and then the total number is discretized by a series of minimal units, which represents the the number of vehicles running in a discrete unit. Figure 11 illustrates the discretization of the total tonnage.

Figure 11: Discretization of the total tonnage

The approach imposes a threshold value on the maximum of the removed material at each discrete step of the procedure. The evaluation of the discrete steps, represents the major difference between the update strategy of wheel and rail. It fits well in following

the behaviour of the wear evolution that could present non-linear characteristics outside the discrete steps. The update strategy includes following operations:

- For each contact step, get the spatial integration of all the wear contributions inside the contact patch, along the longitudinal direction and then get the average value per unit length.
- During a certain time series of simulation, sum all the wear contributions coming from all time-steps to obtain the depth of the removed material. For one time point among the time series, sum the wear contributions coming from all the contact points of a contact pair.
- Amplify the removed material during the dynamic simulations to reduce the simulated track length through a scaling procedure.
- A smoothing procedure is adopted to remove the numerical noise.

The route map of the Metro line is with a length of 12.8 km. The running line adopts four-car articulated driverless trains. The vehicle is modelled in Simpack Rail. The vehicle consists of four carbodies and five bogies. Each bogie consists of 2 wheelsets. The new wheel and the rail profiles in this metro line are the S1002 and UNI50 type. The rails in R260Mn steel and wheels in B6T steel provide the hardness ratio as 0.93. Real profiles of the rails have been measured and implemented as initial rail profiles for simulation. The online recorded running speed file of the vehicle is applied for the vehicle dynamics simulations. Both curving and traction/braking processes have been considered in the simulations. The coefficient of friction is set as 0.3. No flange lubrication is applied. The measurements of the wheel and rail profiles were preformed since August 2015 to January 2016. An interval of 1-2 months during this period was set, and the corresponding travelling distance of the metro is shown in Table 5.

Date	AUG	OCT	NOV	DEC	JAN
Distance [km]	10448	30359	38532	53935	62365

Table 5: Measurement history of the wheel.

Figure 14 shows the measured profiles of first leading wheelset as an example, including the left wheel and the right wheel. The measured profile at different time is distinguished by color. From Figure 14, it is seen that the worn of wheel profile is distributed along the wheel thread, mainly from -800 mm to -710 mm (-50 to 40 mm around the nominal rolling circle).

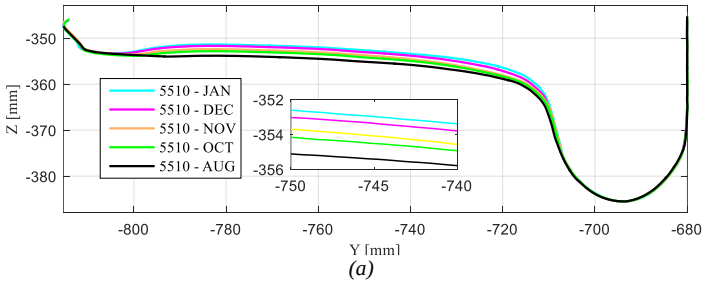

(a)

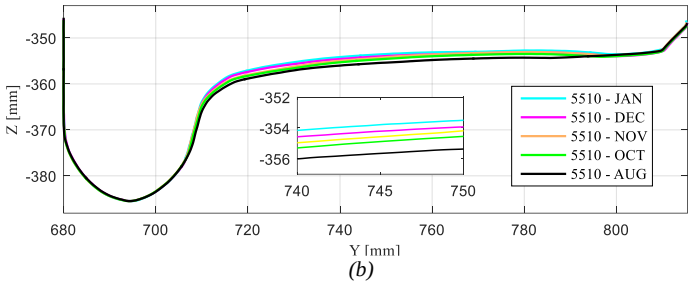

(b)

Figure 14: Measurement: worn profiles of the leading wheelset (a) left wheel (b) right wheel.

According to the measured data, we consider 0.4 mm as the depth value to be used for each of total 7 steps during the procedures of the wheel profile updating. Table 6 lists the recorded monthly temperature in the metro line [12].

Month	Aug	Sep	Oct	Nov	Dec
High [°C]	29	24	18	11	7
Low [°C]	20	16	11	6	2

Table 6: Monthly temperature in the Metro line.

We substitute the monthly average temperature into the formulas 8-9 to get the corresponding K1 values. For those in the severe and catastrophic wear regimes, we assume that the wear rate equals to it when $\frac{T\gamma}{A}$ =25 N/mm^2 . To well compare the prediction and the measurements, the measured profile at the first time (Aug) is taken as the initial profile for the wheel. For the rail, the threshold value is set as 1 mm, and the rail 1 step is set for updating the rail profile. Figures 10(a) and 10(b) show the evolution of the left and the right wheel profiles from the wear prediction model. Figure 15 compares the wheel wear evolution between simulated and measured results after a mileage of around 38000 km. Note that the first leading wheels in the test metro are selected for analysis. The colour in the figure distinguishes different steps during the total steps. It is seen that the worn of wheel profile is distributed along the wheel thread, for the left wheel mainly from -800 mm to -710 mm (-50 to 40 mm around the nominal rolling circle), and for the right wheel from 710 mm to 800 mm. It agrees well with the measured results.

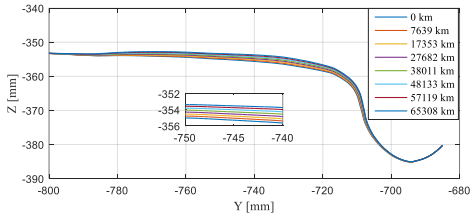

(a)

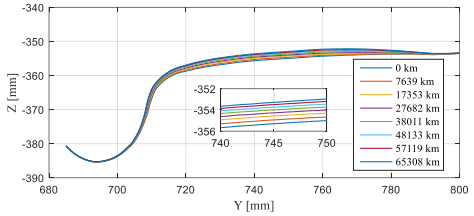

(b)

Figure 15: Simulation: worn profiles of the leading wheelset (a) left wheel (b) right wheel

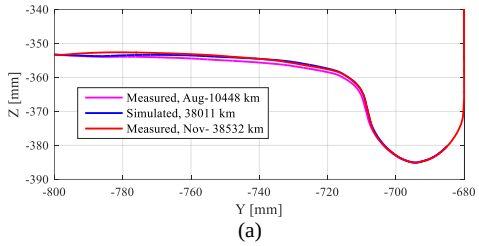

(a)

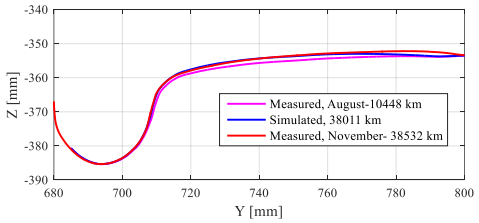

(b)

Figure 16: Comparison of simulated and measured profiles of the leading wheelset (a) left wheel (b) right wheel.

The comparison of maximum wear depth between -40 mm and 40 mm around the nominal rolling circle, from the simulation and the measurements as a function of mileage, is illustrated in Figure 16.

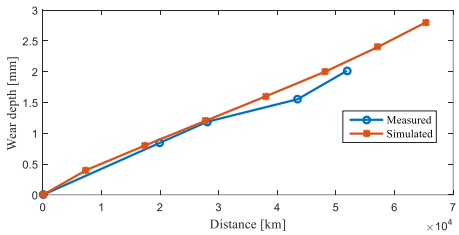

Figure 17: Comparison of wheel wear evolution between simulated and measured results.

It is clear from Figure 17 that the wear of wheel is developed as the mileage is longer. Within around 75,000 km of travel distance, the wear depth increases until around 3 mm. The changing law of the wear depth as a function of mileage agrees well between the measurement and the simulation.The shape of the rail profile in practice is related to its location and the curvature of its location, showing high variety. We have selected one representative, located around 300 m from the Garibaldi station. The measurements are carried out respectively in the month of August and October 2015 (with approximately 20,235 times of passes), which are shown as blue and red solid lines in the Figure 18. It is seen that the difference between two measurements in August and October is, in the region of maximum wear, about 0.8 mm. According to the measured data, we consider 0.26 mm as the depth value to be used for each of total 3 steps during the procedures of the rail profile updating. The results profiles of the left and the right rails from simulation are plotted in Figure 18.

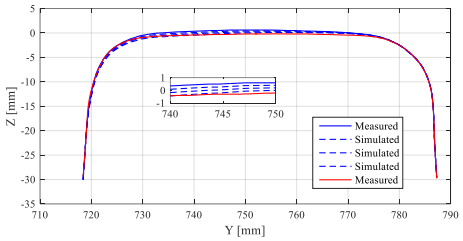

(a)

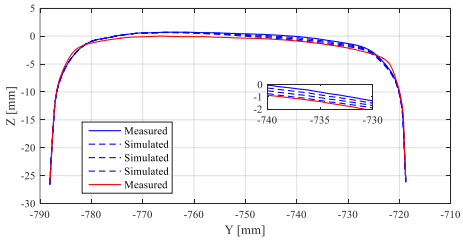

(b)

Figure 18: Rail profile wear results (a) low rail (b) high rail.

From the simulation, the number of metro vehicle passes is estimated as 22309 vehicles, rather close to that of in practice (20,235). By comparing the results from the measurement and the simulation, it is preliminarily proved that the results from the simulation are well consistent with those from field measurements.

5 Conclusions and Contributions

This paper presents the influence of material hardness ratio and ambient temperature on wear modelling. Firstly, wear tests are carried out under various values for the rail/wheel hardness ratio and ambient temperature in the laboratory, providing groups of data related to wear rate for the rail and the wheel. Subsequently, based on the experimental results, the correlation between hardness ratio as well as ambient temperature and worn mass has been analysed, leading to the development of new wear laws. New wear laws are formulated, and the related coefficients are determined, based on USFD law. Proposed new laws have been validated through a numerical example based on a prediction model. The new wear laws would therefore be

applicable for various wheel and rail materials with corresponding hardness ratios, and the corresponding values of ambient temperature.

Acknowledgements

The authors would like to thank the research group of Tribology Research Institute from Southwest Jiaotong University, Chengdu for providing experimental data.

References

[1] M. Meacci, Z. Shi, E. Butini, L. Marini, E. Meli, A. Rindi, A local degraded adhesion model for creep forces evaluation: an approximate approach to the tangential contact problem, Wear 440 (2019) 203084.
[2] R. Lewis, U. Olofsson, Wheel-Rail Interface Handbook, Elsevier, 2009.
[3] Y. Zhu, W. Wang, R. Lewis, W. Yan, S.R. Lewis, H. Ding, A review on wear between railway wheels and rails under environmental conditions, J. Tribol. 141 (12) (2019).
[4] R. Lewis, P. Christoforou, W. Wang, A. Beagles, M. Burstow, S. Lewis, Investigation of the influence of rail hardness on the wear of rail and wheel materials under dry conditions (ICRI wear mapping project), Wear 430 (2019) 383–392.
[5] Y. Zhu, Y. Lyu, U. Olofsson, Mapping the friction between railway wheels and rails focusing on environmental conditions, Wear 324 (2015) 122–128.
[6] Y. Hu, L. Zhou, H. Ding, G. Tan, R. Lewis, Q. Liu, J. Guo, W. Wang, Investigation on wear and rolling contact fatigue of wheel-rail materials under various wheel/rail hardness ratio and creepage conditions, Tribol. Int. 143 (2020) 106091.
[7] Y. Lyu, E. Bergseth, U. Olofsson, Open system tribology and influence of weather condition, Sci. Rep. 6 (1) (2016) 1–11.
[8] L. Ma, L. Shi, J. Guo, Q. Liu, W. Wang, On the wear and damage characteristics of rail material under low temperature environment condition, Wear 394 (2018) 149–158.
[9] L. Ma, W. Wang, J. Guo, Q. Liu, Study on wear and fatigue performance of two types of high-speed railway wheel materials at different ambient temperatures, Materials 13 (5) (2020) 1152.
[10] L. Zhou, Y. Hu, H. Ding, Q. Liu, J. Guo, W. Wang, Experimental study on the wear and damage of wheel-rail steels under alternating temperature conditions, Wear 477 (2021) 203829.
[11] L. Zhou, W. Wang, Y. Hu, S. Marconi, E. Meli, H. Ding, Q. Liu, J. Guo, A. Rindi, Study on the wear and damage behaviors of hypereutectoid rail steel in low temperature environment, Wear 456 (2020) 203365.
[12] Y. Lyu, Y. Zhu, U. Olofsson, Wear between wheel and rail: A pin-on-disc study of environmental conditions and iron oxides, Wear 328 (2015) 277–285.
[13] F. Braghin, R. Lewis, R. Dwyer-Joyce, S. Bruni, A mathematical model to
[14] predict railway wheel profile evolution due to wear, Wear 261 (11–12) (2006) 1253–1264.

[15] J. Pombo, J. Ambrosio, M. Pereira, R. Lewis, R. Dwyer-Joyce, C. Ariaudo, N. Kuka, Development of a wear prediction tool for steel railway wheels using three alternative wear functions, Wear 271 (1–2) (2011) 238–245.
[16] Z. Shi, S. Zhu, A. Rindi, E. Meli, Development and validation of a wear prediction model for railway applications including track flexibility, Wear 486 (2021) 204092.
[17] Z. Shi, L. Nencioni, E. Meli, H. Ding, W. Wang, R. Andrea, Effect of material hardness ratio on wear and rolling contact fatigue: Development and validation of new laws, Wear 514 (2023) 204561.
[18] R. Lewis, U. Olofsson, Mapping rail wear regimes and transitions, Wear 257 (7–8) (2004) 721–729.
[19] R. Lewis, F. Braghin, A. Ward, S. Bruni, R. Dwyer-Joyce, K. Bel Knani, P. Bologna, Integrating Dynamics and Wear Modelling to Predict Railway Wheel Profile Evolution, CHARMEC, 2003.
[20] E. Butini, L. Marini, M. Meacci, E. Meli, A. Rindi, X. Zhao, W. Wang, An innovative model for the prediction of wheel-Rail wear and rolling contact fatigue, Wear 436 (2019) 203025.
[21] National Centers for Environmental Information, 2022, https://www.ncei.noaa.gov/. (Accessed: 30 June 2022).
[22] Shi, Z., Nencioni, L., Meli, E., Ding, H., Wang, W., & Rindi, A. (2024). Effect of ambient temperature on wheel and rail wear: Development and validation of new laws. Wear, 538, 205230.
[23] Shi, Z., Nencioni, L., Meli, E., Ding, H., Wang, W., & Andrea, R. (2023). Effect of material hardness ratio on wear and rolling contact fatigue: Development and validation of new laws. Wear, 514, 204561.
[24] Shi, Z., NENCIONI, L., Meli, E., Wang, W., Ding, H., & Rindi, A. (2022). Effect of ambient temperature for wear on wheels and rails. In 12th International Conference on Contact Mechanics and Wear of Rail/Wheel Systems, 4-7 September 2022, Melbourne, Victoria, Australia.